Journal of Catalysis 417 (2023) 14–21

Contents lists available at ScienceDirect

Journal of Catalysis

journal homepage: www.elsevier.com/locate/jcat

Boosting the propylene selectivity over embryonic borosilicate zeolite catalyst for oxidative dehydrogenation of propane

Bin Qiu, Wen-Duo Lu, Xin-Qian Gao, Jian Sheng, Min Ji, Dongqi Wang, An-Hui Lu *

State Key Laboratory of Fine Chemicals, Liaoning Key Laboratory for Catalytic Conversion of Carbon Resources, School of Chemical Engineering, Dalian University of Technology, Dalian 116024, Liaoning, PR China

ARTICLE INFO

Article history:
Received 26 September 2022
Revised 11 November 2022
Accepted 22 November 2022
Available online 26 November 2022

Keywords:
Embryonic borosilicate zeolite
Reaction kinetics
Gas-phase reaction
ODHP
Propylene

ABSTRACT

Boron-containing zeolites have been proven potential in catalyzing the oxidative dehydrogenation (ODH) process and the boron sites in open coordination are considered as the active center. By considering the diversity and adjustability in the crystal structure of zeolite, there is a great opportunity to further tune the activity and selectivity. Herein, the embryonic borosilicate zeolite with abundant defective sites and developed large porosity is prepared for catalyzing ODH of propane reaction. An ~ 20 % improvement in propylene selectivity is achieved at propane conversion of 21.5 % at 540 °C, with propylene productivity nearly an order of magnitude higher compared with crystalline MFI-type borosilicate zeolite. Solid-state NMR reveals the formation of boron sites in open coordination derived from the defect-rich structure of embryonic borosilicate zeolite, guaranteeing ample exposure of the active center. Combined with kinetic measurements, the reaction in the gas phase initiated by the active boron sites is mainly responsible for the high catalytic performance in ODH of propane reaction. The designed experiment indicates the strengthened gas-phase reaction facilitates the activation of propane, consequently resulting in the increase of reaction order of propane from 1.06 to 2.30. This work reveals the significant role of gas-phase reactions during the ODH of propane reaction and provides a new insight for boosting the propylene selectivity of zeolite-based catalysts.

1. Introduction

Boron-based catalysts have received significant attention for their inhibition of deep oxidation of olefins in the oxidative dehydrogenation of propane (ODHP) process for the production of propylene [1–9]. Recently, boron-containing zeolite catalysts with diversity and adjustability crystal structures are capable of catalyzing ODHP reaction and provide a unique perspective to understand the reaction process and further develop highly active and selective catalysts [10–15]. The aggregated boron species embedded in MWW- and MFI-typed zeolite displayed high efficiency in activating propane [11,13,14]. However, the hydrolysis-prone nature of B—O—B unit in the aggregated boron species tend to raise stability problem of the catalysts in humid atmosphere. The silanol-rich structure was shown to disperse boron species and limit their detachment from the catalytic system through the redispersion of over-hydrolyzed boron species. Lately, the isolated boron site with —B[$OH...O(H)—Si$]$_2$ structure in borosilicate zeolite showed durability in long period test and enabled the synergistic conversion of oxygen and propane through three hydrogen bonds on the boron site [12]. In addition, the selectivity of propylene in zeolite-based catalysts was much lower under identical propane conversion compared with other boron-based catalysts. It was noteworthy that propane reaction orders of 1 and 1.5 were observed in zeolite-based catalysts, suggesting the surface activation of propane was more favourable [12,13]. These results enlightened that the activation of propane on the surface might dominate the ODHP process over zeolite-based catalysts, resulting in the distinctive catalytic properties and distinguishing them from other boron-based catalysts.

For hexagonal boron nitride-based (*h*-BN) and B_2O_3-based catalysts, it is gradually recognized that, in addition to surface-catalyzed pathway, gas-phase radical reactions are also the important issue during the ODHP process, which could influence the overall catalytic activity [8,16–24]. Wu lately reported the improvement of ODHP activity via the gas-phase radical chemistry over VO_x-modified BN catalyst, evidenced by the formation of NO according to the observation of synchrotron vacuum ultraviolet photoionization mass spectroscopy (SVUV-PIMS) [25]. Moreover, a 1.4-order dependent on the propane partial pressure was observed, which was caused by the enhanced surface contribution

* Corresponding author.
E-mail address: anhuilu@dlut.edu.cn (A.-H. Lu).

https://doi.org/10.1016/j.jcat.2022.11.031
0021-9517/

catalyzed by VO_x site. Therefore, it can be reasonably deduced that the lower reaction order of propane and catalytic activity over zeolite-based catalysts could result from the limited contribution of gas-phase reactions. In consideration of the reaction pathways, the construction of highly exposed active boron centers and enhanced gas-phase reactions might be a feasible way to construct highly active and selective ODHP catalysts.

Compared with crystalline zeolite with microporous structure and saturated coordination framework atoms, embryonic zeolitic materials have the feature of extra-large microporosity with several unit cell dimensions of size. The greatly exposed small unit cells allow guest molecules easy to diffuse and the extra-large micropores improve the efficiency of mass transfer and accessibility of the active sites. More importantly, after embedding boron atoms, the defect-rich zeolitic structures offer abundant Si—OH and B—OH groups, which contributed to the stabilization of boron species and construction of active boron centers with proton transfer with adjacent Si—OH through hydrogen bonds. In addition, the large microporous spaces provide free environments for gas-phase reactions, allowing X-ray amorphous zeolitic material as a model system for the fundamental investigation of ODHP reaction.

Herein, the embryonic borosilicate zeolite (EBZ) was prepared and used for investigating the ODHP reaction. Structure characterizations and kinetic measurements revealed that the H-bonded B—OH groups in defect tri-coordination boron species were responsible for activating propane on the catalyst's surface and gas phase, and the reactions in the gas phase were mainly responsible for the high performance in ODHP reaction. The strengthened contribution of gas-phase reaction facilitates the activation of propane, consequently resulting in higher reaction order of propane. It enables the enhanced catalytic performance of embryonic borosilicate zeolite catalyst in terms of propane conversion and propylene selectivity.

2. Experimental methods

2.1. Catalyst preparation

The amorphous embryonic borosilicate zeolite catalysts were synthesized using tetrapropylammonium hydroxide (TPAOH) as organic structure-directing agents (OSDA) from clear homogeneous sols with a molar composition of SiO_2: B_2O_3: TPAOH: H_2O: EtOH = 1: x: 0.14: 21: 4 (x = 0.084, 0.168, 0.252 and 0.336). Typically, boric acid (Sinopharm) was dissolved in 4.8 g aqueous solution of TPAOH (25 wt%, Guangfu) and 24 mL deionized water with stirring at room temperature. Then, 8.68 g tetraethyl orthosilicate (TEOS, Sinopharm) was slowly added to the mixture and strongly stirred for 24 h. Then the gel was filtered, washed, dried by freeze-drying at −50 °C under vacuum, and finally calcined at 550 °C in the air for 6 h to remove the templating agent. The obtained solid product was washed thoroughly with deionized water at 60 °C for 3 h to remove the soluble boron species, then the sample was filtrated, washed with ethanol, dried at 50 °C, and calcined at 550 °C for 2 h in air. The obtained samples were named EBZ-1, EBZ-2, EBZ-3, and EBZ-4, accordingly with B_2O_3: SiO_2 of 0.084, 0.168, 0.252, and 0.336 in the sols. The EBZ-2-AT was prepared by stirring 500 mg EBZ-2 in 25 mL nitric acid (15 mol/L) at 80 °C for 4 h. After cooling down to room temperature, the product was filtered, washed, dried at 120 °C, and finally calcined at 550 °C in air for 2 h.

The crystalline borosilicate MFI-type zeolite (BMFI) was synthesized with similar molar composition of EBZ-2. The resulting homogeneous sol was strongly stirred for 2 h at room temperature, then further hydrothermal treated at 150 °C for 3 days in Teflon-lined stainless-steel autoclave. After cooling down to room temperature, the product was filtered, dried, and finally calcined at 550 °C in air for 6 h to remove the templating agent.

2.2. Catalyst characterization

The actual boron content of the zeolites was measured by inductively coupled plasma optical emission spectroscopy (ICP-OES) on Optima2000DV. Before the measurements, the sample (50 mg) was dissolved by hydrochloric acid (1 mL) and hydrofluoric acid (1 mL) mixed solution in a Teflon-lined autoclave at 150 °C for 1 h. After evaporating up the solution that contained hydrochloric acid and hydrofluoric acid, we repeatedly added deionized water into the Teflon container and then collected the solution into a polypropylene volumetric flask, finally fixed the solution volume as 25 mL.

The powder X-ray diffraction (XRD) was recorded on PANalytical X'Pert3 Powder diffractometer using Cu Kα radiation (λ = 0.15 406 nm). The zeolite powder was placed inside a quartz-glass sample holder for testing. The tube voltage was 40 kV, and the current was 40 mA.

N_2 sorption isotherms were measured with an ASAP 2020 sorption analyzer (Micromeritics). Prior to the measurement, the sample was degassed by evacuation at 200 °C for 6 h. The Brunauer-Emmett-Teller (BET) method was used to calculate the specific surface area (S_{BET}). Total pore volume (V_{total}) was calculated from the amount of gas adsorbed at a relative pressure P/P_0 of 0.99. Micropore volume (V_{micro}) was calculated using the *t*-plot method. The micro-mesopore size distribution was extracted from density functional theory modeling of the adsorption branch.

Thermogravimetric (TG) analysis was performed on STA 449 F3 (NETZSCH) in air atmosphere with a heating rate of 10 °C/min from room temperature to 800 °C. Prior to analysis, the catalysts were pre-treated with flowing Ar (40 mL/min) at 200 °C for 2 h, and then cooled to ambient temperature. The CO_2 generated was monitored by online mass spectrometry (MS).

Fourier transform infrared spectroscopy (FTIR) spectra were recorded on a Nicolet 6700 FT-IR spectrometer equipped with a mercury cadmium telluride (MCT) detector. *In-situ* Diffuse Reflectance Infrared Fourier Transform (DRIFT) spectra were collected on a Bruker 70 V spectrometer equipped with an *in-situ* reaction cell (HARRICK) and MCT detector. The catalyst powder (∼30 mg) was placed in the cell and pretreated at 530 °C for 2 h in a flow of Ar. Subsequently, the sample was maintained at 500 °C in flowing $C_3H_8/O_2/Ar$ (volume ratio of 1.5:1:2.5) gas mixture. The evolution of surface species was monitored by IR by averaging 256 scans at a resolution of 4 cm^{-1}.

^{11}B MAS NMR spectra were recorded on Agilent DD2-500 MHz spectrometer with an 11.7 T magnet, using a 4-mm MAS NMR probe with a spinning rate of 10 kHz. The spectra were acquired with 600 scans per increment, a recycle delay of 3 s. Chemical shifts were referenced to a 1 M H_3BO_3 aqueous solution at 19.6 ppm.

^{29}Si MAS NMR spectra were recorded at 99.3 MHz, using a 6-mm MAS NMR probe with a spinning rate of 4 kHz. The spectra were acquired with 500 scans per increment, a recycle delay of 4 s. Kaolin was used as the chemical shift reference.

2.3. Catalytic tests of propane oxidative dehydrogenation

Selective oxidation of propane was studied in a fixed bed reactor (I. D. = 8 mm, length = 420 mm, treated with nitric acid) packed with 100 mg catalyst (without diluent, 40–60 mesh) in the middle of reactor and heated to 490–550 °C under atmospheric pressure. The feed gas contains $C_3H_8/O_2/N_2$ with a volume ratio of 1.5:1:2.5 at a weight-hour-space-velocity (WHSV) of 5.3 g_{C3H8} g_{cat}^{-1}-h^{-1}. Before reaction, each EBZ catalyst was pretreated to stabilize

the coordination environment of boron species under reaction conditions. Reactants and products were analyzed using an online gas chromatograph (Techcomp, GC 7980) equipped with a GDX-102 and molecular sieve 5A column. A TCD was used to detect O_2, N_2, C_3H_8, C_3H_6, C_2H_4, CO, and CO_2. H_2 was not detected in EBZ catalysts. Conversion was defined as the number of moles of carbon converted divided by the number of moles of carbon present in the feed. Selectivity was defined as the number of moles of carbon in the product divided by the number of moles of carbon reacted. The carbon balance was checked by comparing the number of moles of carbon in the outlet stream to the number of moles of carbon in the feed. Under our typical evaluating conditions, the carbon balance was generally higher than 95 %.

The controlled homogeneous gas-phase reactions of propane were performed under the same experimental conditions, except for packing quartz sand (40–60 mesh) to fill the empty volume of the reactor on both sides of the catalyst bed. The free space distance after the catalyst was adjusted to ~ 0, ~5, ~10, and ~ 25 mm for modulating the gas-phase reaction.

The mass and heat transfer diffusion limitations have been ruled out for the highest propane reaction rate based on the Weisz-Prater criterion and Mears criterion [26,27] as shown in Supplementary Material.

The reaction rate of propane $r(C_3H_8)$ was calculated as follows:

$$r(C_3H_8) = F(C_3H_8) \times X(C_3H_8) / m(cat).$$

where $F(C_3H_8)$ is the molar flow rate of C_3H_8 at the inlet of the reactor, $X(C_3H_8)$ represents the conversion of C_3H_8, and m(cat) is the weight of the catalyst.

3. Results and discussion

3.1. Structure and property of EBZ catalysts

The structure and property of EBZ catalysts were characterized and the results were shown in Fig. 1. All the harvested EBZ catalysts showed X-ray amorphous nature and no typical diffraction peaks of MFI were observed (Fig. 1a), due to the size of several zeolite units below the detection limit by XRD. FTIR was used to characterize the short-range orders of the EBZ catalysts. As seen in Fig. 1b, the absorption bands around 1080 and 800 cm^{-1} correspond to the asymmetric and symmetric Si—O stretching vibration. The absorption band at around 570 and 1225 cm^{-1} were generally attributed to the stretching vibration of double rings and external asymmetric stretching of the MFI structure [28]. The N_2 sorption isotherms of the solid were displayed in Fig. 1c. For EBZ catalysts, a type Ib isotherm was observed with a significant uptake at low relative pressure followed by smooth sorption branches at P/P_0 < 0.1, which ensued from extra-large micropores [29]. Besides, a second uptake at the range of P/P_0 = 0.7–1.0 originated from the textural generated by the small zeolite nanocrystals could be observed for the EBZ catalysts except for EBZ-1. As summarized in Table S1, the S_{BET} and surface area of micropore negatively correlated with the B/Si ratio in the sols (S_{BET}: from 771 to 426 m^2/g, S_{micro}: from 737 to 126 m^2/g), indicating that the degree of structural order decreased with increased amount of boric acid used. The micropore size distribution curve of EBZ-1 showed two broad peaks with maximum at 0.6 and 1.2 nm, which was smaller than other EBZ catalysts (0.9 and 1.4 nm, Fig. 1d). Moreover, all the EBZ catalysts showed mesoporous with pore width of 2–10 nm. These results suggested that the EBZ catalysts with hierarchical structure could be obtained through regulating the B/Si ratio in the sols.

The TG-MS was used to further insight into the structure of the EBZ catalysts. As shown in Fig. 1e, f, the TG curves and corresponding CO_2 MS signals displayed two stages of weight loss. The first stage in the range of 300–400 °C was attributed to the relatively weak interactions between the cations and borosilicate species probably located on the surface of zeolitic units. The temperature range greater than 400 °C corresponded to the decomposition of TPA^+ that has been occluded inside the zeolitic units [30,31]. Moreover, the weight loss of EBZ-1 and EBZ-2 catalysts was higher than that of the other catalysts, demonstrating the strong structure-directing ability of the OSDA at a B/Si ratio below 0.168 in sols. In literature, the introduction of boron into the growth medium can promote the aggregation of silica sols, leading to the formation of spherical particulates that seemingly assemble via a combination of aggregation, densification (ripening), and growth processes [32]. However, when the boron content in the sols exceeded from one specific amount, depending on the synthesis conditions, the crystallization of borosilicate was hampered and the framework boron content decreased. Therefore, the catalysts showed

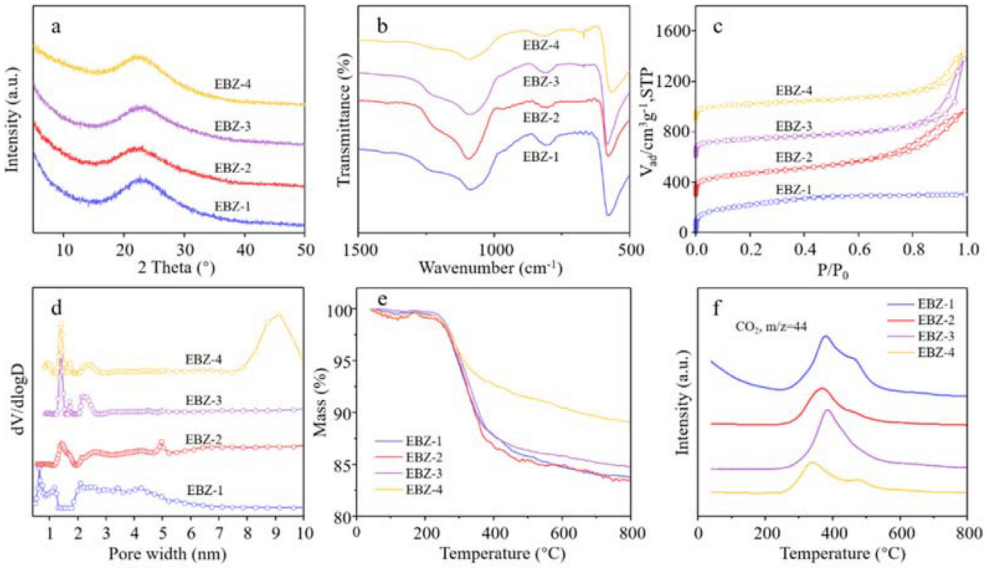

Fig. 1. (a) XRD patterns, (b) FTIR spectra, (c) N_2 sorption isotherms, and (d) pore size distributions of the EBZ catalysts. N_2 sorption isotherms of EBZ-2, EBZ-3, and EBZ-4 were vertically shifted an additional 250, 600, and 900 $cm^3\ g^{-1}$ (STP) for easy view. (e) TG curves and (f) corresponding CO_2 MS signals of EBZ catalysts.

mesoporous-microporous hierarchical structure when the B/Si ratio was above 0.168 in the synthesis process and a decrease in boron content when the B/Si ratio reached 0.332.

3.2. Catalytic performance of EBZ catalysts

The catalytic activity of the EBZ catalysts for ODHP reaction was conducted using a reaction gas consisting of C_3H_8, O_2, and N_2 in molar ratios of 1.5:1:2.5, at a total WHSV of 5.3 $g_{C3H8}\ g_{cat}^{-1}h^{-1}$. The blank experiment with quartz sand under identical conditions showed propane conversion of only 0.7 %, evidencing that the EBZ catalysts were essential for catalyzing the ODHP reaction (Figure S1). As shown in Fig. 2a and Table S2, the amorphous EBZ catalysts showed considerable propane conversion and much superior propylene selectivity compared to the conventional microporous BS-1 zeolite catalyst at higher WHSV [12]. The EBZ-1, EBZ-2, and EBZ-3 catalysts exhibited nearly identical propane conversion of 21.4 %, 21.5 %, and 19.7 % at 540 °C, respectively. While a lower propane conversion of 13.7 % for EBZ-4 was observed. The difference in propane conversion is ascribed to the boron content of the EBZ catalysts. As the main product, the propylene selectivity for EBZ-2 is 73.5 %, similar to EBZ-3 (72.7 %) and slightly higher than EBZ-1 (68.4 %) (Figure S2). Therefore, the molar ratio of B/Si = 0.168 was the optimal choice for the synthesis of high-performance EBZ catalysts in the present study. Fig. 2b showed the temperature dependence of propane conversion and corresponding product distribution over the EBZ-2 catalyst. Higher temperatures afford higher propane conversions, and the propane conversions rapidly increased when the temperatures were above 530 °C. For example, as the temperature was increased from 500 to 530 °C, the propane conversion increased from 1.9 % to 9.8 %. And 23.7 % of propane conversion was achieved when the reaction temperature further increased to 540 °C. The EBZ-2 catalyst showed higher selectivity towards propylene of 73.5 % and propylene productivity of 0.80 $g_{C3H6}\ g_{cat}^{-1}h^{-1}$ at 540 °C, which is superior to the crystalline borosilicate MFI-type zeolite catalyst [12]. In addition, the EBZ-2 catalyst still exhibited promising propylene selectivity and productivity under the same reaction conditions as in the literature (Table S2). The EBZ-1 and EBZ-2 catalysts also showed good stability with a constant propane conversion of ~ 20 % at 540 °C for 30 h (Fig. 2c, d; Figure S3).

3.3. Clarification of the origin of catalytic activity

The structural information of the calcined EBZ catalysts was provided by [29] Si MAS NMR spectra, as shown in Fig. 3a. Two resonance bands centered at −103 and −113 ppm were observed, which were ascribed to the tetrahedrally coordinated silicon in Q3 ($(SiO)_3Si—OH$) and Q4 ($Si(OSi)_4$) microenvironments. It was worth noting that the EBZ catalysts showed higher ratio of Q3 and broader resonance band of Q4 compared with crystalline BMFI. These results suggested the presence of incompletely crystallized zeolite framework and defect-rich structure of EBZ catalysts.

Considering that EBZ-2 catalyst exhibited the optimum catalytic activity, we selected the EBZ-2 catalyst for further investigation of the origin of catalytic activity. Firstly, ^{11}B solid-state NMR was conducted to explore the boron species of the EBZ-2 catalyst. As shown in Fig. 3b, the signals were in the range of above 0 ppm, indicating that all the boron species were tricoordinated. In consideration of the solubility of the boron species, the relative stable structure of trigonal boron species in the catalyst after washing could be B$(OSi)_3$ (donated as B[3]I) [8,11]. It may also include the hydrolysis products of $B(OSi)_3$, i. e., $B(OSi)_2(OH)$ or $B(OSi)(OH)_2$ (donated as B[3]II) [12]. The existence of these boron species can be verified by the signals at ~ 10 and ~ 15 ppm. Compared with conventional crystalline zeolite, the EBZ-2 catalyst offered additional unsaturated coordination boron sites in the framework, which might contribute to the enhancement of the ODHP activity. It was noteworthy that the signals in ^{11}B MAS NMR before and after ODHP reaction were almost the same, confirming the good cat-

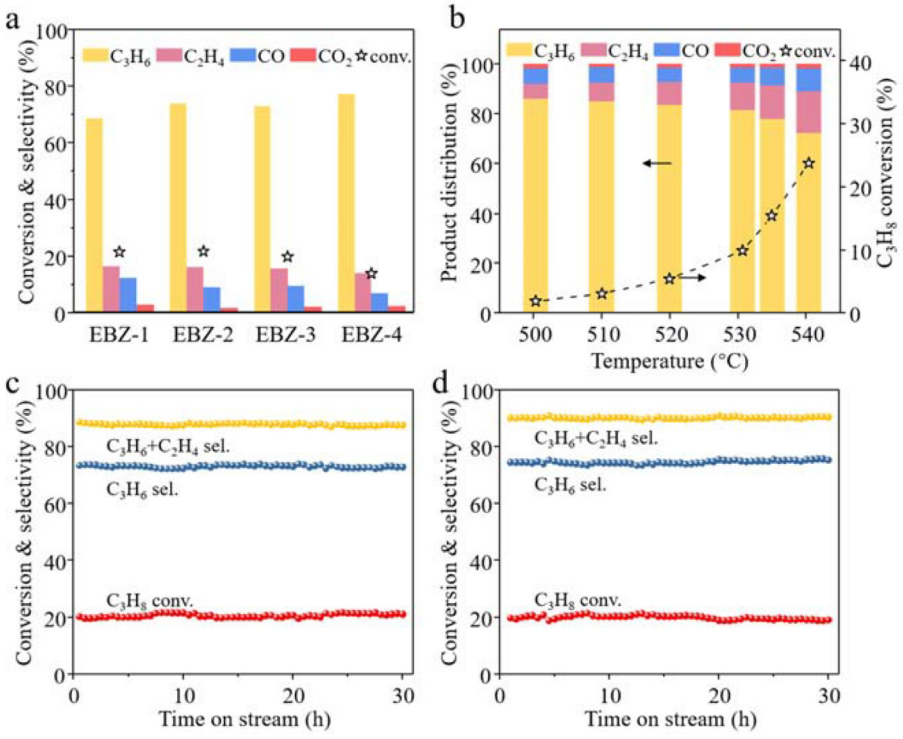

Fig. 2. (a) Propane conversion and product distribution at 540 °C on EBZ catalysts. (b) Effect of reaction temperature on C_3H_8 conversion and corresponding product distribution of EBZ-2 catalyst. (c, d) Stability test during 30-h operation over EBZ-1 and EBZ-2 catalysts at 540 °C.

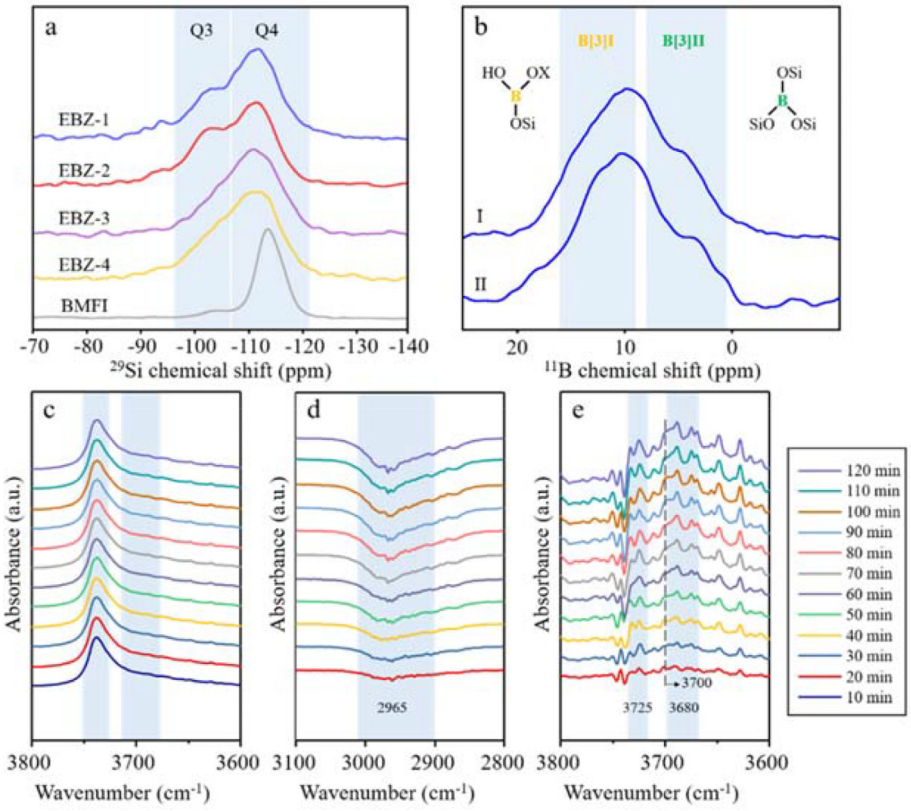

Fig. 3. (a) ^{29}Si MAS NMR spectra of calcined EBZ catalysts and crystalline BMFI zeolite. (b) ^{11}B MAS NMR spectra of (I) fresh and (II) spent EBZ-2 catalyst, X = H or Si. (c) *In-situ* DRIFT spectra of fresh EBZ-2 catalyst and (d, e) the difference spectra under C_3H_8/O_2/Ar atmosphere at 500 °C.

alytic stability of the EBZ-2 catalyst. These results indicated that a certain portion of trigonal boron species stably anchored in the framework of EBZ-2 catalyst after washing with water. These boron species might be the active centers for the ODHP reaction.

Furthermore, *in-situ* DRIFT measurements were conducted to monitor the structure evolution of the EBZ-2 catalyst and clarification the origin of catalytic activity (Fig. 3c-e). The spectra contained a broad peak at 3740 cm^{-1} and a shoulder at 3700 cm^{-1} that corresponded to external Si—OH and isolated B—OH vibrations, respectively [33,34] (Fig. 3c). The signal at 2965 cm^{-1} was the alkyl stretching vibrations that attributed to the gas-phase propane [35]. Upon exposure to the ODHP conditions, a continuous decline of the alkyl stretching signal in ~ 2965 cm^{-1} was observed, suggesting an enhancement in the reaction rate of propane (Fig. 3d). Meanwhile, the vibrations at 3725 cm^{-1} and 3680 cm^{-1} increased, which were assigned to the internal Si—OH and hydrogen-bonded B—OH [36,37] (Fig. 3e). Notably, although the broad band of 3680 cm^{-1} overlapped with the band at 3700 cm^{-1}, it was reasonable to conclude that both bands were increasing in intensity with the promotion of the reaction rate of propane. To further verify the origin of the hydroxyl groups, the EBZ-2 catalyst was washed with nitric acid to remove the boron sites, and the corresponding *in-situ* DRIFT difference spectra under C_3H_8/O_2/Ar atmosphere were shown in Figure S4. During the 120-minute measurement, no changes on the surface structure of the catalyst and gas-phase propane occurred, confirming the increased intensity of the bands of 3700 and 3680 cm^{-1} were derived from the B—OH groups. These results suggested that the boron species underwent hydrolysis of the B—O—Si bond with the help of water during the ODHP reaction, generating more B—OH groups that afforded a higher reaction rate of propane. In addition, the boron atoms were located within the micropore structure other than on the external surface of the embryonic zeolite matrix, since only the silanol groups in the internal surface were generated. As a result, some boron sites were hydrogen-bonded with adjacent silanol groups. A similar phenomenon was also observed for the EBZ-1 catalyst (Figure S5), indicating the presence of identical active boron species of EBZ catalysts. Lately, the hydrogen bond between B—OH and adjacent Si—OH was found to facilitate the synergistic conversion of oxygen and propane through decreasing energy barriers in ODHP reaction [12]. In addition, it also resulted in the oxygen atom at B – OH being more nucleophilic and assisted the dehydrogenation of B – OH with O_2 by stabilizing the transition state with a reduced reaction barrier. The formed B – O· was highly active in the hydrogen abstraction of propane and was able to trigger the subsequent surface and gas phase dehydrogenation processes [23]. Therefore, the B—OH groups, especially the hydrogen-bonded B—OH in defect trigonal boron sites played the role of activating propane, which is responsible for the catalytic activity of ODHP reaction over EBZ catalysts.

3.4. Kinetic behavior of EBZ catalysts

Kinetic experiments were performed to gain insights into the reaction behavior of propane ODH over the EBZ-1 and EBZ-2 catalysts. For EBZ-2 catalysts, the effect of propane partial pressure on the ODHP reaction showed near third-order dependence on propane concentration, which was higher than the reported boron-based catalysts (Fig. 4a). In addition, a first-order dependence of the propane reaction rate for oxygen partial pressure was observed (Fig. 4b). Similar results were obtained for the EBZ-1 catalyst, indicating that the EBZ catalysts shared similar kinetic characteristics but are different from other boron-based catalysts (Figure S6). Moreover, the influence of residence time on the propane conver-

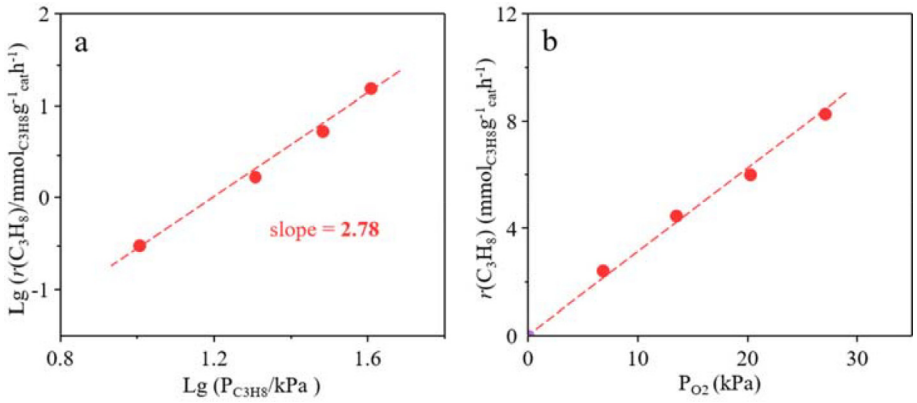

Fig. 4. Dependence of reaction rate on (a) C_3H_8 and (b) O_2 partial pressure of ODHP over EBZ-2 catalyst at 520 °C, m_{cat} = 100 mg, P_{O2} constant at 20 kPa and P_{C3H8} constant at 30 kPa, N_2 balance.

sion was evaluated, as shown in Figure S7. Different from the linear trend of the propane conversion with residence time over lithium-promoted magnesia catalyst [38]. The propane conversion increased almost linearly with the residence time at the range of 0.2–0.7 s, while following an exponential curve at high residence time on EBZ-2 catalysts. In the previous reports, the secondary dependence of propane partial pressure on ODHP reaction over boron-based catalysts was believed to involve surface and gas-phase radical reactions [8,19–22]. Lately, a first-order rate dependence with respect to propane partial pressure was obtained at the BS-1 catalyst, suggesting the ODHP reaction mainly occurred on the surface of the BS-1 catalyst [12]. Therefore, the higher reaction dependence of propane and oxygen partial pressure may arise from the enhanced contribution of gas-phase activation of propane during the oxidative dehydrogenation process.

We performed controlled homogeneous gas-phase reactions in ODHP over EBZ-2 to elucidate the effects of gas-phase reactions by modulating the distance of downstream quartz sand away from the catalyst bed as 0, 5, 10, and 25 mm (Figure S8). Fig. 5a showed the propane reaction rate as a function of propane partial pressure at a given value of O_2 partial pressure. A propane reaction order of 1.06 was obtained when there was no free space downstream of the catalyst bed, indicating that the propane was activated mainly on the surface of the catalyst. Furthermore, the reaction order of propane increased to 1.50 and 1.91, respectively, when the interspace distance between the catalyst bed and quartz sand was adjusted to 5 and 10 mm, indicating the propane could be activated in the gas phase when free space existed downstream of the catalyst bed, and larger free space was conducive to the gas-phase reaction. Since a pool of radicals needs to be formed to autocatalytically accelerate the reactions [38]. Regarding the dependence of oxygen partial pressure on the reaction rate (Fig. 5b), the reaction order was 0.24, 0.30, and 0.48, respectively, for 0-, 5-, and 10-mm interspace distance in the control experiments. These results suggested that molecular oxygen was also involved in the activation of propane in the gas phase over EBZ catalysts. When the interspace distance was modulated to 25 mm, further increases in propane (2.30) and oxygen (0.50) partial pressures were observed at 520 °C (Figure S9). Therefore, we can then deduce that the high reaction order of propane resulted from the contribution of the activation of propane in the gas phase.

Furthermore, we evaluated the propane conversion and the product distribution of ODHP under the control conditions. As shown in Fig. 5c and Figure S10, the propane conversion and propylene selectivity were 1.2 % and 60.8 % at the interspace distance of 0 mm under 540 °C. Except for light olefins, CO_2 and CO were the main by-products with a selectivity of 28.6 %. When the quartz sand was loaded 5 and 10 mm below the catalyst bed, an increase in propane conversion was observed at evaluated temperatures. Moreover, the selectivity toward propylene was also improved and the CO_x selectivity was greatly reduced. For example, a propylene selectivity of 76.9 % was obtained with CO_x selectivity of 9.1 % at 540 °C when the distance of interspace was set to 10 mm. Furthermore, the propane conversion further enhanced to 12.5 % at an interspace distance of 25 mm, which is 10 times higher than no free space downstream of the catalyst bed. When the reactor was not filled with quartz sand to maximize the free space of gas-phase reactions, the EBZ-2 catalysts exhibited the highest propane conversion and propylene selectivity (Figure S11). And showed more than 8 times of olefin productivity compared with crystalline MFI borosilicate zeolite (Table S2). It is worth noting that the propylene selectivity increased with propane conversion at interspace distances of 0, 5, and, 10 mm in the controlled experiments, which was opposite to that when unloaded with quartz sand. This could be due to the increased proportion of propane activation in the gas phase at rising temperatures, as the reaction rate of gas-phase reactions was much dependent on the reaction temperature (Fig. 5d). A similar phenomenon was also observed for the EBZ-1 catalyst except for a lower propylene selectivity (Figure S12). The activation of propane was supposed to mainly occur on the surface of catalysts when a first-order dependence of reaction rate on propane partial pressure was observed. Accordingly, the contribution of gas-phase reactions on the ODHP process was estimated to be 20 %, 53 %, and, 90 %, respectively, for 5-, 10-, and, 25-mm interspace distances. It was about 94 % when the catalyst was loaded without quartz sand, indicating the significant enhancement of gas-phase reactions toward propane activation and propylene selectivity control.

As known, metal-based catalysts displayed high reactivity toward the oxidative conversion of propane in ODHP reaction while suffering from serious over-oxidation of propylene to CO_x, causing loss of olefin products. Some works have shown that high yields of propylene and ethylene can be obtained through combining a catalytic reaction with a post-catalyst homogeneous reaction. Burch and Crabb showed that the maximum selectivity to propylene at a specific propane conversion for the oxide-based catalysts (V/MgO, Li/MgO, MoV, et. al) was lower than can be obtained in the absence of a catalyst [39,40]. Furthermore, Nguyen and Kung reported that a propane conversion of 17 % was achieved at a propylene selectivity of 53 % in a conventional packed-bed reactor over V/MgO catalyst. When a void volume was present downstream from the catalyst bed, the propane conversion increased to 69 % accompanied by the selectivity decreased to 37 % [41]. With the help of modeling study, the surface-enhanced homogeneous

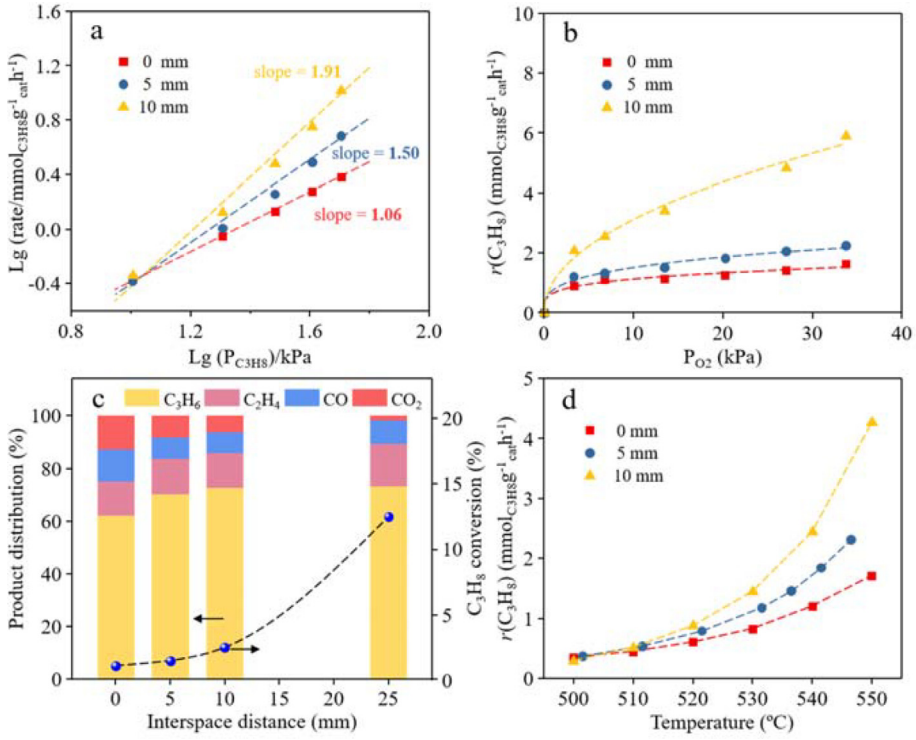

Fig. 5. (a, b) Dependence of reaction rate on C_3H_8 (P_{O2} constant at 20 kPa) and O_2 (P_{C3H8} constant at 30 kPa) partial pressure. (c) C_3H_8 conversion and product distribution at 540 °C, and (d) Dependence of propane reaction rate on the temperature of EBZ-2 catalyst under controlled homogeneous gas-phase reactions of ODHP.

reaction involving gas-phase reactions initiated by the desorption of reactive intermediates from a catalyst surface was proposed [41,42]. Therefore, the coupling of the heterogeneous system to activate propane and homogeneous decomposition of desorbed radical species to propylene was believed to be the better conditions for obtaining high productivity of propylene in the ODHP process [43].

For EBZ-2 catalysts, the enhancement in propane conversion and propylene selectivity could be rationalized in terms of the co-play of surface and gas-phase reactions of propane oxidation. The activation of propane on the boron-based catalyst was reported to happen at the surface boron sites with adsorbed oxygen [8,23]. During this process, the B—O· could be obtained through hydrogen abstraction from B—OH by dioxygen, and the hydrogen bond with adjacent Si—OH groups were able to reduce the reaction barrier of this process. Meanwhile, the hydroperoxo (HO_2·) radicals could be formed accompanied by the generation of B—O·. After abstracting the first hydrogen of C_3H_8, the HO_2· and C_3H_6 could be formed through rapid hydrogen donation from C_3H_7·to an oxidative species in its vicinity, e. g. an O_2 molecule (C_3H_7· + O_2 → C_3H_6 + HO_2·, $\Delta G^{\neq}$ = 15.0 kcal/mol, ΔG = −13.0 kcal/mol) [8,23]. In our previous report, the nascent B—O· and HO_2· were highly reactive under ODH conditions towards the activation of propane on the surface and in the gas phase, respectively (C_3H_8 + BO· → C_3H_7· + BOH, $\Delta G^{\neq}$ = 4.5 kcal/mol, ΔG = −15.1 kcal/mol; C_3H_8 + HO_2· → C_3H_7· + H_2O_2, $\Delta G^{\neq}$ = 22.1 kcal/mol, ΔG = 18.6 kcal/mol) [23]. Therefore, the formed radical species can serve as additional "active centers" in the gas phase and higher post-bed volume provided more gas-phase "active centers", contributing to the significant increase in propane conversion. Hence, we may conclude that both surface and gas-phase reactions are involved in the ODHP process over EBZ catalysts (Fig. 6), and the enhancement in surface-initiated gas-phase radical reactions contribute to the improvement of catalytic activity and propylene productivity.

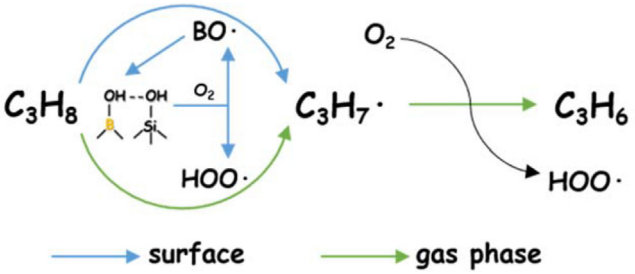

Fig. 6. The proposed reaction pathways of ODHP for EBZ catalysts.

4. Conclusions

In this work, the embryonic borosilicate zeolite catalyst with small zeolite units, developed porosity, and active boron species was prepared by using TPA^+ as the organic structure directing agent for catalyzing ODHP reaction. Such catalyst was convenient to prepare and showed ~ 20 % improvement in propylene selectivity at propane conversion of 21.5 % at 540 °C and displayed nearly an order of magnitude higher of propylene productivity compared with crystalline MFI-type borosilicate zeolite. From the combination of ^{11}B MAS NMR and *in-situ* DRIFT, the H-bonded B—OH groups in the EBZ catalysts were presently identified as the active sites for the activation of propane and triggering the gas-phase reactions. Kinetic measurement revealed that the gas-phase reactions showed a significant role for the high ODHP performance. The designed experiment indicated the strengthened contribution of gas-phase reaction facilitated the activation of propane, consequently resulting in the increase of reaction order of propane from 1.06 to 2.30. This work provides an ideal model for fundamentally understanding the scientific foundation behind their remarkable

efficiency in ODHP performance, consequently facilitating the deployment of active and selective ODH zeolite-based catalysts.

Data availability

No data was used for the research described in the article.

Declaration of Competing Interest

The authors declare that they have no known competing financial interests or personal relationships that could have appeared to influence the work reported in this paper.

Acknowledgements

This study was supported by state key program of National Natural Science Foundation of China (21733002), National Key Research and Development Program of China (2018YFA0209404), the Program for Liaoning Innovative Research Team in University (LT2016001).

Appendix A. Supplementary material

Supplementary data to this article can be found online at https://doi.org/10.1016/j.jcat.2022.11.031.

References

[1] J.M. Venegas, W.P. McDermott, I. Hermans, Serendipity in Catalysis Research: Boron-Based Materials for Alkane Oxidative Dehydrogenation, Acc. Chem. Res. 51 (2018) 2556–2564.
[2] L. Shi, Y. Wang, B. Yan, W. Song, D. Shao, A.-H. Lu, Progress in selective oxidative dehydrogenation of light alkanes to olefins promoted by boron nitride catalysts, Chem. Commun. 54 (2018) 10936–10946.
[3] J. Sheng, B. Yan, W.-D. Lu, B. Qiu, X.-Q. Gao, D. Wang, A.-H. Lu, Oxidative dehydrogenation of light alkanes to olefins on metal-free catalysts, Chem. Soc. Rev. 50 (2020) 1438–1468.
[4] J.T. Grant, C.A. Carrero, F. Goeltl, J. Venegas, P. Mueller, S.P. Burt, S.E. Specht, W. P. McDermott, A. Chieregato, I. Hermans, Selective oxidative dehydrogenation of propane to propene using boron nitride catalysts, Science 354 (2016) 1570–1573.
[5] R. Huang, B. Zhang, J. Wang, K.-H. Wu, W. Shi, Y. Zhang, Y. Liu, A. Zheng, R. Schlögl, D.S. Su, Direct Insight into Ethane Oxidative Dehydrogenation over Boron Nitrides, ChemCatChem 9 (2017) 3293–3297.
[6] L. Shi, D. Wang, W. Song, D. Shao, W.-P. Zhang, A.-H. Lu, Edge-hydroxylated Boron Nitride for Oxidative Dehydrogenation of Propane to Propylene, ChemCatChem 9 (2017) 1788–1793.
[7] L. Cao, P. Dai, J. Tang, D. Li, R. Chen, D. Liu, X. Gu, L. Li, Y. Bando, Y.S. Ok, X. Zhao, Y. Yamauchi, A Spherical Superstructure of Boron Nitride Nanosheets Derived from Boron-Contained Metal-Organic Frameworks, J. Am. Chem. Soc. 142 (2020) 8755–8762.
[8] W.-D. Lu, D. Wang, Z. Zhao, W. Song, W.-C. Li, A.-H. Lu, Supported Boron Oxide Catalysts for Selective and Low-Temperature Oxidative Dehydrogenation of Propane, ACS Catal. 9 (2019) 8263–8270.
[9] Q. Liu, Y. Wu, F. Xing, Q. Liu, X. Guo, C. Huang, B_2O_3@BPO_4 sandwich-like hollow spheres as metal-free supported liquid-phase catalysts, J. Catal. 381 (2020) 599–607.
[10] N. Altvater, R. Dorn, M. Cendejas, W. McDermott, B. Thomas, A. Rossini, I. Hermans, B-MWW Zeolite: The Case Against Single-Site Catalysis, Angew. Chem. Int. Ed. 59 (2020) 6546–6550.
[11] B. Qiu, F. Jiang, W.-D. Lu, B. Yan, W.-C. Li, Z.-C. Zhao, A.-H. Lu, Oxidative dehydrogenation of propane using layered borosilicate zeolite as the active and selective catalyst, J. Catal. 385 (2020) 176–182.
[12] H. Zhou, X. Yi, Y. Hui, L. Wang, W. Chen, Y. Qin, M. Wang, J. Ma, X. Chu, Y. Wang, X. Hong, Z. Chen, X. Meng, H. Wang, Q. Zhu, L. Song, A. Zheng, F.-S. Xiao, Isolated boron in zeolite for oxidative dehydrogenation of propane, Science 372 (2021) 76–80.
[13] B. Qiu, W.-D. Lu, X.-Q. Gao, J. Sheng, B. Yan, M. Ji, A.-H. Lu, Borosilicate zeolite enriched in defect boron sites boosting the low-temperature oxidative dehydrogenation of propane, J. Catal. 408 (2022) 133–141.
[14] B. Gao, B. Qiu, M. Zheng, Z. Liu, W.-D. Lu, Q. Wang, J. Xu, F. Deng, A.-H. Lu, Dynamic Self-Dispersion of Aggregated Boron Clusters into Stable Oligomeric Boron Species on MFI Zeolite Nanosheets under Oxidative Dehydrogenation of Propane, ACS Catal. 12 (12) (2022) 7368–7376.
[15] R.W. Dorn, M.C. Cendejas, K. Chen, I. Hung, N.R. Altvater, W.P. McDermott, Z. Gan, I. Hermans, A.J. Rossini, Structure Determination of Boron-Based Oxidative Dehydrogenation Heterogeneous Catalysts With Ultrahigh Field 35.2 T ^{11}B Solid-State NMR Spectroscopy, ACS Catal. 10 (23) (2020) 13852–13866.
[16] K. Otsuka, Y. Uragami, T. Komatsu, M. Hatano, The Partial Oxidation of Light Alkanes (CH_4,C_2H_6,C_3H_8) over B-P Mixed Oxides, Nat. Gas Convers. (1991) 15–23.
[17] J. Tian, J. Tan, M. Xu, Z. Zhang, S. Wan, S. Wang, J. Lin, Y. Wang, Propane oxidative dehydrogenation over highly selective hexagonal boron nitride catalysts: The role of oxidative coupling of methyl, Sci. Adv. 5 (2019) eaav8063.
[18] W.P. McDermott, J. Venegas, I. Hermans, Selective Oxidative Cracking of *n*-Butane to Light Olefins over Hexagonal Boron Nitride with Limited Formation of CO_x, ChemSusChem 13 (2020) 152–158.
[19] J.M. Venegas, I. Hermans, The Influence of Reactor Parameters on the Boron Nitride-Catalyzed Oxidative Dehydrogenation of Propane, Org. Process Res. Dev. 22 (2018) 1644–1652.
[20] J.M. Venegas, Z. Zhang, T.O. Agbi, W.P. McDermott, A. Alexandrova, I. Hermans, Why Boron Nitride is such a Selective Catalyst for the Oxidative Dehydrogenation of Propane, Angew. Chem. Int. Ed. 59 (2020) 16527–16535.
[21] X. Zhang, R. You, Z. Wei, X. Jiang, J. Yang, Y. Pan, P. Wu, Q. Jia, Z. Bao, L. Bai, M. Jin, B. Sumpter, V. Fung, W. Huang, Z. Wu, Radical Chemistry and Reaction Mechanisms of Propane Oxidative Dehydrogenation over Hexagonal Boron Nitride Catalysts, Angew. Chem. Int. Ed. 59 (2020) 8042–8046.
[22] P. Kraus, R.P. Lindstedt, It's a Gas: Oxidative Dehydrogenation of Propane over Boron Nitride Catalysts, J. Phys. Chem. C. 125 (2021) 5623–5634.
[23] Z. Liu, W.-D. Lu, D. Wang, A.-H. Lu, Interplay of On- and Off-Surface Processes in the B2O3-Catalyzed Oxidative Dehydrogenation of Propane: A DFT Study, J. Phys. Chem. C 125 (2021) 24930–24944.
[24] Z. Liu, D. Xu, M. Xia, W.-D. Lu, A.-H. Lu, D. Wang, Understanding the Unique Antioxidation Property of Boron-Based Catalysts during Oxidative Dehydrogenation of Alkanes, J. Phys. Chem. Lett. 12 (2021) 8770–8776.
[25] X. Jiang, X. Zhang, S.C. Purdy, Y. He, Z. Huang, R. You, Z. Wei, H.M. Meyer, J. Yang, Y. Pan, P. Wu, W. Zhu, M. Chi, K. Page, W. Huang, Z. Wu, Multiple Promotional Effects of Vanadium Oxide on Boron Nitride for Oxidative Dehydrogenation of Propane, JACS Au 2 (2022) 1096–1104.
[26] D.E. Mears, Diagnostic Criteria for Heat Transport Limitations in Fixed Bed Reactors, J. Catal. 20 (1971) 127–131.
[27] X. Fan, D. Liu, X. Sun, X. Yu, D. Li, Y. Yang, H. Liu, J. Diao, Z. Xie, L. Kong, X. Xiao, Z. Zhao, Mn-doping induced changes in Pt dispersion and Pt_xMn_y alloying extent on Pt/Mn-DMSN catalyst with enhanced propane dehydrogenation stability, J. Catal. 389 (2020) 450–460.
[28] J.C. Jansen, F.J. van der Gaag, H. van Bekkum, H.van Bekkum, Identification of ZSM-type and other 5-ring containing zeolites by i.r. spectroscopy, Zeolites 4 (4) (1984) 369–372.
[29] M. Thommes, K. Kaneko, A.V. Neimark, J.P. Olivier, F. Rodriguez-Reinoso, J. Rouquerol, K.S.W. Sing, Physisorption of gases, with special reference to the evaluation of surface area and pore size distribution (IUPAC Technical Report), Pure and Applied Chemistry 87 (2015) 1051–1069.
[30] R. Bai, M.T. Navarro, Y. Song, T. Zhang, Y. Zou, Z. Feng, P. Zhang, A. Corma, J. Yu, Titanosilicate zeolite precursors for highly efficient oxidation reactions, Chem. Sci. 11 (2020) 12341–12349.
[31] M. Akouche, J.-P. Gilson, N. Nesterenko, S. Moldovan, D. Chateigner, H.E. Siblani, D. Minoux, J.-P. Dath, V. Valtchev, Synthesis of Embryonic Zeolites with Controlled Physicochemical Properties, Chem. Mater. 32 (2020) 2123–2132.
[32] R. Li, A. Chawla, N. Linares, J.G. Sutjianto, K.W. Chapman, J.G. Martínez, J.D. Rimer, Diverse Physical States of Amorphous Precursors in Zeolite Synthesis, Ind. Eng. Chem. Res. 57 (2018) 8460–8471.
[33] M.B. Sayed, A. Auroux, J.C. Védrine, The Effect of Boron on ZSM-5 Zeolite Shape Selectivity and Activity II. Coincorporation of Aluminium and Boron in the Zeolite Lattice, J. Catal. 116 (1989) 1–10.
[34] J. Datka, Z. Piwowarska, OH Groups in Boralites, J. Chern. Soc. Faraday Trans. 1 (85) (1989) 837–841.
[35] G. Liu, Z.-J. Zhao, T. Wu, L. Zeng, J. Gong, Nature of the Active Sites of VO_x/Al_2O_3 Catalysts for Propane Dehydrogenation, ACS Catal. 6 (2016) 5207–5214.
[36] C.T-W. Chu, C.D. Chang, Isomorphous Substitution in Zeolite Frameworks. 1. Acidity of Surface Hydroxyls in [B]-, [Fe]-, [Ga]-, and [Al]-ZSM-5, J. Phys. Chem. 89 (1985) 1569–1571.
[37] H. Koller, C. Fild, R.F. Lobo, Variable anchoring of boron in zeolite beta, Micropor. Mesopor. Mat. 79 (2005) 215–224.
[38] L. Leveles, K. Seshan, J.A. Lercher, L. Lefferts, Oxidative conversion of propane over lithium-promoted magnesia catalyst: I. Kinetics and mechanism, J. Catal. 218 (2003) 296–306.
[39] R. Burch, E.M. Crabb, Homogeneous and heterogeneous contributions to the oxidative dehydrogenation of propane on oxide catalysts, Appl. Catal. A- Gen. 100 (1993) 111–130.
[40] R. Burch, E.M. Crabb, Homogeneous and heterogeneous contributions to the catalytic oxidative dehydrogenation of ethane, Appl. Catal. A- Gen. 91 (1993) 49–65.
[41] K.T. Nguyen, H.H. Kung, Analysis of the Surface-Enhanced Homogeneous Reaction during Oxidative Dehydrogenation of Propane over a V-Mg-O Catalyst, Ind. Eng. Chem. Res. 30 (1991) 352–361.
[42] K.T. Nguyen, H.H. Kung, Generation of gaseous radicals by a V-Mg-O catalyst during oxidative dehydrogenation of propane, J. Catal. 122 (1990) 415–428.
[43] F. Cavani, F. Trifirò, The oxidative dehydrogenation of ethane and propane as an alternative way for the production of light olefins, Catal. Today 24 (1995) 307–313.